Characterization of a Honeycomb-Like Scaffold With Dielectrophoresis-Based Patterning for Tissue Engineering

Zhijie Huan, *Student Member, IEEE*, Henry K. Chu, *Member, IEEE*, Jie Yang, and Dong Sun*, *Fellow, IEEE*

Abstract—Objective: Seeding and patterning of cells with an engineered scaffold is a critical process in artificial tissue construction and regeneration. To date, many engineered scaffolds exhibit simple intrinsic designs, which fail to mimic the geometrical complexity of native tissues. In this study, a novel scaffold that can automatically seed cells into multilayer honeycomb patterns for bone tissue engineering application was designed and examined. ***Methods***: The scaffold incorporated dielectrophoresis for noncontact manipulation of cells and intrinsic honeycomb architectures were integrated in each scaffold layer. When a voltage was supplied to the stacked scaffold layers, three-dimensional electric fields were generated, thereby manipulating cells to form into honeycomb-like cellular patterns for subsequent culture. ***Results***: The biocompatibility of the scaffold material was confirmed through the cell viability test. Experiments were conducted to evaluate the cell viability during DEP patterning at different voltage amplitudes, frequencies, and manipulating time. Three different mammalian cells were examined and the effects of the cell size and the cell concentration on the resultant cellular patterns were evaluated. ***Conclusion***: Results showed that the proposed scaffold structure was able to construct multilayer honeycomb cellular patterns in a manner similar to the natural tissue. ***Significance***: This honeycomb-like scaffold and the dielectrophoresis-based patterning technique examined in this study could provide the field with a promising tool to enhance seeding and patterning of a wide range of cells for the development of high-quality artificial tissues.

***Index Terms*—Cell patterning, cell viability, dielectrophoresis, Scaffold.**

Z. Huan is with the Department of Precision Machinery and Instrumentation, University of Science and Technology of China, and also with the Department of Mechanical and Biomedical Engineering, City University of Hong Kong.

H. K. Chu was with the Department of Mechanical and Biomedical Engineering, City University of Hong Kong. He is now with the Department of Mechanical Engineering, The Hong Kong Polytechnic University.

J. Yang is with the Department of Precision Machinery and Instrumentation, University of Science and Technology of China.

*D. Sun is with the Department of Mechanical and Biomedical Engineering, City University of Hong Kong, Kowloon, Hong Kong (e-mail: medsun@cityu.edu.hk).

I. INTRODUCTION

TISSUE engineering is an interdisciplinary research that aims to repair and regenerate tissues and organs by transplanting artificial tissues fabricated outside the human body. To construct these tissues, one common approach is to harvest stem cells from the bone marrow of the patient and then culture these cells on a biomaterial as the scaffold to facilitate tissue development [1], [2]. Thus, the scaffold acts as the 3-D platform mimicking the structural characteristics of the native tissue for cells to adhere, proliferate, and differentiate. Various biomimetic scaffolds have been proposed for reconstructing different functional tissues [3], [4]. Nevertheless, many of these scaffolds exhibit relatively simple intrinsic designs with limited control of cell distribution throughout the scaffold. In addition, manipulating and migrating cells to the interior regions of the scaffold remains technically challenging because cell seeding efficiency highly depends on the microarchitecture of the scaffold. The conventional, passive method could take hours for cell seeding, and the cell distribution may not be uniform. The use of vacuum to rapidly seed cells into the scaffold is another method, but the effects on the cells and the scaffold are not clear [5]. The microfluidic method could precisely define the cell pattern to be constructed, but the size of the pattern is constrained by the microfluidic chip and the pattern is relatively two-dimensional (2-D) [6].

A number of techniques have been identified to manipulate a large group of cells for biomedical applications over the past decades. For instance, optical tweezers use highly focused laser beams to exert trapping forces on the dielectric particles for manipulation [7]–[10]. However, the damage induced by the trapping laser on the cell, also known as photodamage [11], may need to be considered [12], [13]. Magnetic cell manipulation uses magnetic fields to remotely manipulate magnetic nanoparticles attached to cell surfaces. When the magnetic nanoparticles are coated with an antibody that can only attach to a particular cell type, high-throughput sorting of targeted cells from a mixed cell sample can be achieved [14], [15]. The biocompatibility and the toxicity of the nanoparticles need to be considered when using this technique for tissue regeneration. Other manipulation techniques based on the mechanical properties of cells have also been investigated [16], [17].

Dielectrophoreis (DEP) is the movement of cells in nonuniform electric fields, caused by the induced dipole moment of the cells. Combined with microfabrication technology, DEP has been widely used in cell sorting, trapping, fractionation,

and cytometry [18]. DEP has also been used in tissue engineering to create different cellular patterns for culture and tissue development. Examples of these patterns include dot array [19], [20], linear [21], [22], radial [23]–[25], and interdigitated patterns [26]. Hydrogels are often used as the substrate for immobilizing the cells, thereby allowing the use of the patterned cells for subsequent culture. Owing to the relatively soft nature of these gels, their applications are mainly focused on soft tissue regeneration.

In the present study, DEP was used as the mechanism to promote cell seeding during the reconstruction of an artificial bone tissue. Achieving a high density of spatially distributed cells on a 3-D scaffold is an essential process as it can lead to the disposition of more homogeneous extracellular matrix by cells, enhancing the quality and functionality of the tissues to be developed [27]. Cells on the scaffold are automatically patterned into multiple layers of honeycomb patterns so as to mimic the architecture and complexity of native tissues for improved tissue culture performance [28].

Stainless steel is considered as the scaffold material as it is commonly used as the implanting material to replace damaged bone or support bone healing [29]. In addition to its comparable tensile strength to natural bones [30], stainless steel can provide excellent electrical conductivity, which is an essential material property in the present work. Although metallic scaffolds could be prone to corrosion due to wear, surface medication or coating could be used to overcome some of these disadvantages. The proposed metallic scaffold consists of multiple layers that serve as microelectrodes to generate the required electric fields for cell manipulation. In contrast to conventional scaffolds with a uniform grid pattern or woven pore architecture, including that in our earlier study [31], this scaffold was designed with honeycomb-like pores to mimic the geometry of native bone tissues. When a voltage was supplied to the scaffold, the DEP effect induced the suspending cells to manipulate and adhere to the multilayer scaffold, thereby forming multiple honeycomb cellular patterns for culture. In [32], a preliminary design of the honeycomb-like scaffold structure was reported and yeast cells were examined with the scaffold as a proof of concept. In the present study, we extend our research to the characterization of the proposed scaffold on a number of aspects. First, three different mammalian cells were considered and different factors affecting the formation of the honeycomb patterns were identified by experimentation. Computer simulation was performed to evaluate the optimal frequency with respect to the cell type for patterning. Viability tests were conducted to examine to the biocompatibility of the material and the cell death associated with the DEP mechanism.

II. MATERIALS AND METHODS

A. Principle of DEP

DEP is among the most widely used methods for cell manipulation because of its noninvasiveness and ease of implementation. The application of DEP has been significantly developed since its discovery by Pohl [33]. The DEP force is the interaction of a nonuniform electric field with the dipole moment induced on a polarizable particle. For a spherical isotropic homogenous particle, the time-averaged DEP force is given by Jen and Chen [34], as follows:

$$\langle F_{\text{DEP}} \rangle = 2\pi \varepsilon_m r^3 \text{Re}\left[f_{\text{CM}}(\omega) \right] \nabla \left| \vec{E} \right|^2 \qquad (1)$$

where ε_m is the real part of the permittivity of the suspending medium, r is the radius of the particle, $\nabla|\vec{E}|^2$ is the gradient of the square of the electric field, and $\text{Re}[f_{\text{CM}}(\omega)]$ is the real part of the Clausius–Mossotti (CM) factor for a spherical object (bounded between -0.5 and 1). The CM factor is expressed as follows:

$$f_{\text{CM}}(\omega) = \frac{\varepsilon_c^*(\omega) - \varepsilon_m^*(\omega)}{\varepsilon_c^*(\omega) + 2\varepsilon_m^*(\omega)} \qquad (2)$$

where $\varepsilon_c^*(\omega)$ and $\varepsilon_m^*(\omega)$ represent the complex permittivity of the cell and the medium.

The complex permittivity is related to the permittivity (ε), the conductivity (σ), and the angular frequency ($\omega = 2\pi f$) of the applied electric field. For mammalian cells, the dielectric properties can be formulated by the protoplast model. The CM factor for live cells can be rewritten [34] as follows:

$$f_{\text{CM}}(\omega) = -\frac{\omega^2 (\tau_m \tau_c^* - \tau_c \tau_m^*) + j\omega(\tau_m^* - \tau_m - \tau_c^*) - 1}{\omega^2 (2\tau_m \tau_c^* + \tau_c \tau_m^*) - j\omega(\tau_m^* + 2\tau_m + \tau_c^*) - 2} \qquad (3)$$

where $\tau_c^* = c_m r/\sigma_c$ and $\tau_c = \varepsilon_m/\sigma_c$ are the time constants for the cell. c_m is the membrane capacitance. σ_c and ε_c are the conductivity and permittivity of the cell, respectively. $\tau_m^* = c_m r/\sigma_m$ and $\tau_m = \varepsilon_m/\sigma_m$ are the time constants for the medium. σ_m and ε_m are the conductivity and permittivity of the medium, respectively. When the cell dies, the cell membrane becomes permeable. The CM factor for dead cells can be rewritten as follows [34]:

$$f_{\text{CM}}(\omega) = \frac{\varepsilon_c - \varepsilon_m - j(\sigma_c - \sigma_m)/\omega}{\varepsilon_c + 2\varepsilon_m - j(\sigma_c + 2\sigma_m)/\omega}. \qquad (4)$$

In accordance with the CM factor, the cell is either trapped or repelled by the induced DEP force. If the cell is more polarizable than the medium, the CM factor becomes positive, and the cell is attracted toward the high electric field gradient region known as the positive DEP (p-DEP). By contrast, if the CM factor is negative, the cell is repelled to the electric field minimum region called the negative DEP or n-DEP.

Both positive and negative DEP phenomena have been employed extensively to manipulate or pattern cells by using electrode pairs with different geometries or configurations [35]–[37]. The key requirement is that electric field maxima or minima should be generated in the microenvironment so that cells are directed to the designated regions accordingly. This study proposed the development of a 3-D multilayer scaffold to generate the nonuniform electric field, and the p-DEP mechanism was applied to attract cells toward the scaffold to form 3-D cellular patterns.

B. Scaffold Design

To enable cell attachment and tissue ingrowth, the scaffold used for tissue repair or regeneration usually has a porous architecture with interconnected pores [38], [39]. The pore can be randomly distributed or precisely controlled depending on the
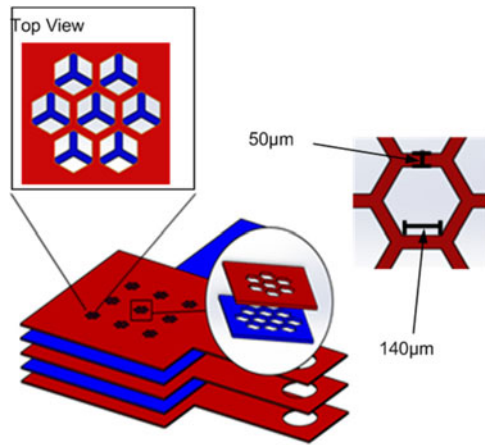
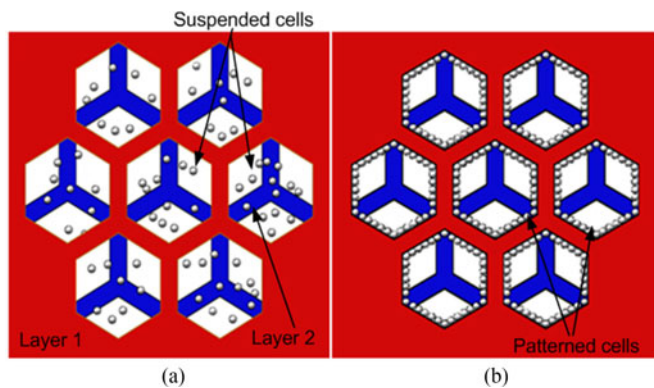Fig. 1. Schematic of the multilayer scaffold.

Fig. 2. Operating principle of cell patterning.

Fig. 3. Electric field simulation of the multilayer structure with 10-V input in (a) 3-D and (b) 2-D [32].

fabrication technique. Recent studies indicated that compared with conventional scaffolds, scaffolds with honeycomb architectures can more efficiently enhance cell proliferation, viability, and survival rate [40]. Honeycomb architectures can more efficiently mimic the morphology of the native bone tissue while providing good mechanical stability to guide tissue formation [41], [42].

In the current study, a 3-D honeycomb-like scaffold prototype consisting of five individual layers was designed and fabricated. To utilize DEP for cell patterning, a voltage opposite to the adjacent layers was applied to each layer so that electrode pairs formed, thereby generating nonuniform electric fields for DEP cell manipulation. Fig. 1 illustrates the schematics of the scaffold. The scaffold layers connected to the positive terminal of the sinusoidal function generator are shown in red, whereas those connected to the ground terminal are shown in blue.

Fig. 2 presents the operating principle of the cell-patterning technique on one layer of the scaffold. When a cell droplet was pipetted onto the scaffold, the pores of the scaffold were filled with randomly distributed cells, as illustrated in Fig. 2(a). When voltage was supplied to the scaffold, nonuniform electric fields were established in the microenvironment, where the gradients are highest at the boundaries of the honeycomb patterns. The suspending cells were polarized and manipulated
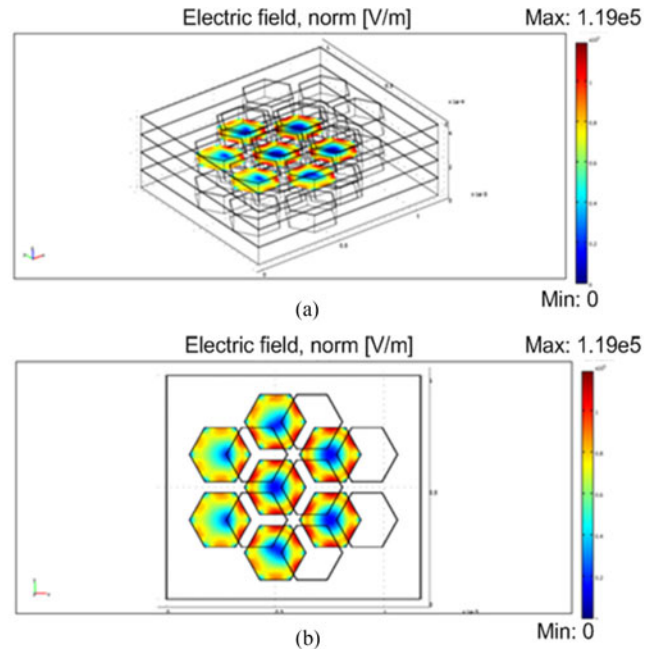
toward the electrode layer to form honeycomb patterns, as shown in Fig. 2(b).

To confirm the efficiency of the honeycomb patterns of the multilayer scaffold for DEP cell manipulation, the finite element software COMSOL was used to simulate the electric field strength and distribution at 10-V voltage input. The simulation results presented in Fig. 3 indicate that the current layer can be paired with the adjacent layers to establish highly nonuniform electric fields. Similar simulation results (data not shown) were obtained at different layers of the scaffold. Based on the p-DEP effect, cells migrated from the lower electric field regions (in blue) and were manipulated toward the higher electric field regions (in red), thereby forming honeycomb-like cellular patterns.

C. Fabrication

Polymeric scaffolds are widely used in tissue engineering because they possess excellent biocompatibility, ease of fabrication, and controllable mechanical properties [43]–[45]. Nevertheless, the elastic moduli of polymers are much lower than those of natural bone tissues. Hence, the use of metallic materials in hard tissue engineering is preferable because of their strength and ability to withstand compressive loads from daily activities after implantation [46]–[48]. Metallic scaffolds are also suitable for current applications because they exhibit high electrical conductivity, which can minimize Joule heating and voltage drop. In the present study, medical stainless steel was chosen to fabricate the multilayer scaffold because of its mechanical properties, biocompatibility, and corrosion resistance [49]. The electrical conductivity of the stainless steel is 1.4×10^4 s/cm.

To construct the multilayer scaffold, rectangular 10 mm $\times$ 10 mm scaffold layers were cut from the stainless steel by
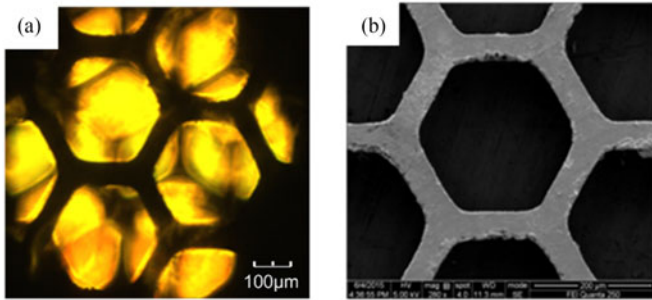
Fig. 4. (a) Microscope image and (b) SEM image of the fabricated scaffold structure.

Fig. 5. DEP manipulation system for cell patterning: (a) inverted microscope; (b) assembled chip; and (c) function generator.

using a commercial GSI laser machine. On each layer, multiple honeycomb patterns were cut, with a positioning accuracy of 5 μm. The length and the width of the honeycomb pattern are 140 and 50 μm, respectively, with a mean pore size of 140 μm. Studies have indicated mean pore sizes ranging from 96 to 150 μm to facilitate optimal attachment in bone tissue engineering [50], [51]. The material was 50 μm thick to reduce mismachining tolerance during laser cutting. Each layer was coated with a 1-μm-thick silica by plasma-enhanced chemical vapor deposition to provide electrical insulation between layers that are stacked together to form a 3-D scaffold. This coating could also enhance cell adhesion during seeding. Fig. 4(a) and (b) presents the microscope image and the scanning electron microscope (SEM) image of the stacked multilayer scaffold, respectively.

D. Cell Culture

Both adherent and suspension mammalian cells were examined for seeding onto the multilayer scaffold. MC3T3-E1 cells are preosteoblast cells derived from mouse calvaria. Human foreskin fibroblasts (HFFs) were isolated from neonatal human foreskin. These two kinds of adherent cells were cultured in 35-mm Petri dishes in Dulbecco's modified Eagle's medium (DMEM) containing 10% (v/v) heat-inactivated fetal bovine serum (FBS) and 1% (v/v) penicillin–streptomycin. Leukemia cells (OCI-AML3) are suspension cells obtained from peripheral blood extracted from a patient. The cells were cultured using Alpha-MEM with 20% FBS and 1% penicillin–streptomycin. All dishes were incubated at 37 °C with a gas mixture of 95% air and 5% CO_2; the culture media were changed every two days. The diameters of HFF, MC3T3-E1, and OCI-AML3 were approximately 20, 15, and 5 μm, respectively, as measured using an optical microscope.

E. Cell Preparation for DEP Manipulation

The two culture media (DMEM and Alpha-MEM) used for the experiments exhibited high conductivity because of high salt concentration, which made them unsuitable for DEP manipulation. A low-conductivity medium (8.5% sucrose, 0.3% dextrose, 20 mg/L $CaCl_2$), which was less polarizable than the cells and could provide the necessary osmotic balance to the cells, was used as the DEP buffer medium to enhance the p-DEP force [52]. Prior to the experiment, MC3T3-E1 and HFF
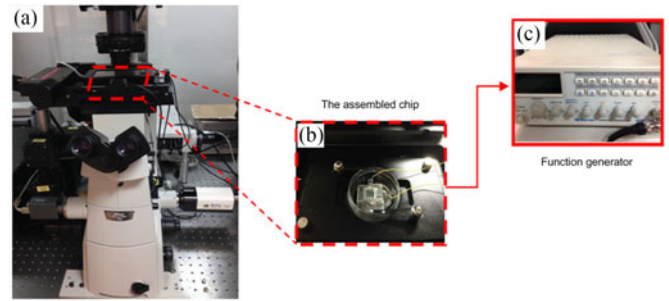
were harvested from the dishes after 90% confluency was obtained. The cells were washed with phosphate-buffered saline (PBS) and then trypsinized using a 0.25% trypsin–EDTA solution. The cells were then detached from the Petri dishes and then transferred to centrifuge tubes to obtain the cell pellets. For suspension OCI-AML3 cells, the cell-containing medium was directly transferred into a centrifuge tube. The cells were resuspended in the DEP buffer medium at different concentrations.

F. Experimental Setup for DEP-Based Cell Patterning

The entire experiment was performed on a vibration isolation table to minimize the influence of the external environment, as illustrated in Fig. 5. The movement and the distribution of the cells during DEP patterning was observed using the Eclipse Ti inverted microscope from Nikon. Images were captured via a digital CCD camera connected to a computer. The stacked multilayer scaffold structure was enclosed by two pieces of PDMS that were bonded together via a plasma bonding machine to form a chamber. The entire structure was bonded on a 35-mm Petri dish and mounted on the stage-top incubator of the inverted microscope. The sinusoidal voltage input applied to the scaffold was provided by a functional generator (GW Instek, GFG8255A) with a maximum voltage of 10 V and a frequency range from 0 to 5 MHz. Prior to the experiments, the scaffold was sterilized with 70% ethanol for 30 min and then placed under UV light for 2 h to allow the scaffold to dry.

III. RESULTS AND DISCUSSION

A series of experiments were conducted to examine the performance of cell manipulation via DEP with the proposed 3-D honeycomb scaffold. First, the operating frequency range that can maximize the induced DEP force was evaluated through simulation. Second, cell viability was examined based on two aspects: the biocompatibility of the selected material for scaffold fabrication and the rate of cell lysis with the patterning time. Finally, the cellular patterns constructed from the proposed scaffold were assayed, and the effects of cell size and concentration on the resultant pattern were examined.

A. Effect of the Frequency of Input Voltage

As discussed in Section II, the sign of the CM factor depends on the frequency of the voltage input. To ensure the maximum
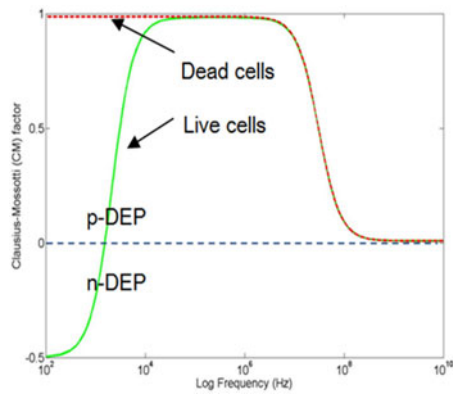
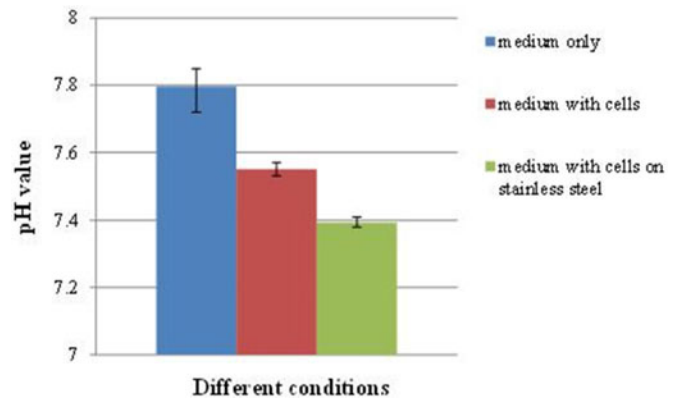Fig. 6. CM values for bone cells in sucrose medium at different frequencies.

Fig. 7. pH values of the culture media after three days under different conditions.

TABLE I
PROPERTIES OF BONE CELLS

Parameter	Value
cell radius (r)	7.5 μm
membrane capacitance (c_m)	1.72 F/cm^2
Cell conductivity	0.4 S/m
Cell permittivity	80 ε_0
Medium conductivity	1.76×10^{-3} S/m
Medium permittivity	78ε_0

Fig. 8. Cell concentrations (cells/mL) after days of culture.

DEP force to be generated for cell manipulation via p-DEP, the CM factor should be set at a value close to 1. In accordance with (3) and (4), the value of the CM factor for MC3T3-E1 (bone) cells in a sucrose medium was plotted using MATLAB, as shown in Fig. 6. The properties of the cells for simulation are summarized in Table I [34], [53]–[55]. The result clearly reveals that a frequency range between 100 kHz and 1 MHz can yield the maximum CM value. A higher frequency input can weaken the DEP force, whereas a lower frequency input can change the DEP effect from positive to negative. Based on the simulated result, a voltage frequency of 500 kHz, which can provide the maximum CM value, was considered throughout the experiments.

B. Effect of the Material on the Cell Culture

A material selected for cell culture in vitro is immersed in the medium for a certain period. Metallic scaffolds can potentially react with the culture medium and release toxic substances to the medium. In this context, three groups of samples were prepared in a 24 well-culture plate, and the pH values of the medium were measured for analysis. If the material degrades, the metal ions react with water to form metal hydroxide, thereby increasing the pH values [48]. For the first group, only the culture medium was added to the wells and then used as the control. For the next two groups, MC3T3-E1 cells from mouse were seeded onto the wells. A piece of the fabricated scaffold layer was immersed in the last group to examine the interaction between the material and the culture medium. The pH values obtained from the three groups after three days of culture are shown in Fig. 7.
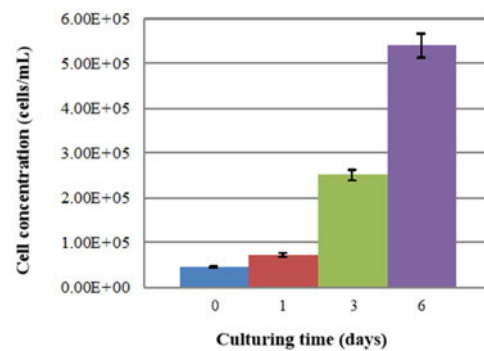
The results reveal that the pH values from groups 2 and 3 are lower than group 1 (control), indicating the metabolic activity of cells during the culture. Nevertheless, the pH value itself may not conclude that the material is relatively inert and optimal for in vitro cell culture. Other factors such as the material hardness could also influence the condition and the metabolism of the cells.

To examine the cell-material interaction, MC3T3-E1 cells were also seeded to the surface of the scaffold layer in the well for culture. The initial cell concentration was measured, and the concentrations after one, three, and six days of culture were measured. As illustrated in Fig. 8, the cell concentration was increased from 4.5×10^4 cells/mL to near 9×10^4 cells/mL after one day of culture. This doubling time is similar to the others findings in the literature, e.g., 20 h in [56]. Cells on the material continued to grow and proliferated exponentially after three and six days of culture.

The scaffold layer after 6 days of culture was inspected under the SEM. The cell seeded layer was fixed with 4% paraformaldehyde, and the layer was dried with an automated Critical Point Dryer (Leica EM CPD300). The layer was coated with 10 nm of gold using a sputter coater (Quorum Q150TS) to make the sample conductive for SEM imaging. Fig. 9 illustrates the SEM images of the cultured layer at different magnifications. After six days of culture, the surface was mostly covered with cells, with some of them found near the edges of the layer.
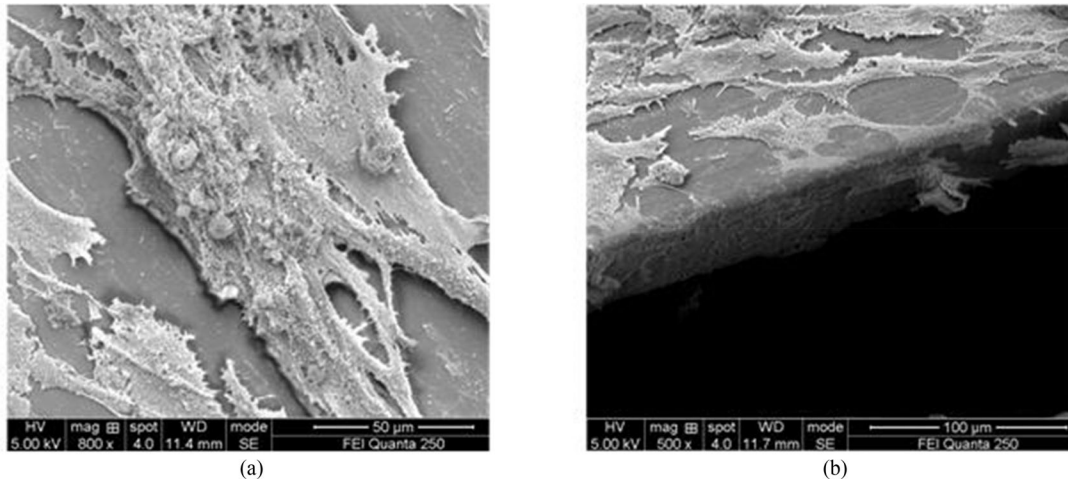
Fig. 9. SEM images of the cultured cells on the structure after six days at (a) high magnification and (b) low magnification.
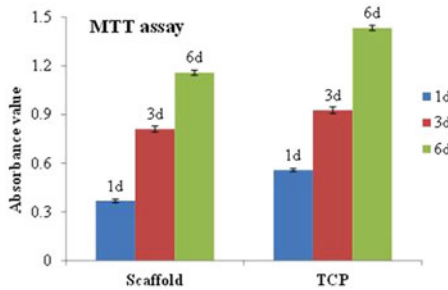

Fig. 10. MTT assay result of MC3T3-E1 cells on the scaffold and a TCP at three different time points.

To further quantify the biocompability of the scaffold material, MTT (3-(4,5-dimethylthiazol-2-yl)-2, 5-diphenylte trazolium bromide) assay was adopted to examine the viability and proliferation of cells as cultured on the material. The assay was conducted according to the ISO 10993-5 standard. During the culture process, MTT is taken up by cells due to its net positive charge and the plasma membrane potential. The amount of formazan produced is related to the number of living cells. A multiwell tissue culture plate (TCP) was used as the control group and compared with the scaffold material. After one, three, and six days of culture, five samples were collected from each group and they were washed with PBS to remove the unattached cells. Then, MTT solution was added to each well at a concentration of 0.5 mg/mL. The culture plate was further incubated for 4 h in the dark in 37 °C. Afterward, the culture medium was aspirated carefully to prevent distribution of the cell monolayer and 600 μL of Formazan Solubilization solution was added in each well to dissolve the formazan crystals. The absorbance of this solution was measured at 570 nm using a microplate reader. The final absorbance was shown as mean value $\pm$ standard deviation in Fig. 10. According to ISO 10993-5, the reduction of cell viability in samples compared to the blank (medium only) after six days of culture is calculated as follows:

$$\text{Viab.}\% = \frac{100 \times OD_{570e}}{OD_{570b}} \qquad (5)$$

where OD_{570e} is the mean value of the measured optical density of the 100% extracts of the test sample, which is 1.158; OD_{570b} is the mean value of the measured optical density of the blank, which is 1.434.

The calculated viability is 80.7%, which is more than 70% of the blank. The material is not cytotoxic according to the ISO standard.

The presented data in Fig. 10 can also be used to evaluate the metabolic activity of the cells cultured on the scaffold material. After six days of culture, the cellular activity continues to increase over time; however, the rate is not as high as the control group. One possible reason could be due to the surface of the material [57]. The scaffold material used for the experiment is untreated and stiffer, whereas the culture plate has a coating which is more favorable for cell attachment and culture. To enhance the culture performance, the scaffold material could be coated with hydroxyapatite or polyvinyl alcohol [58].

C. Cell Viability During DEP Patterning

To perform cell patterning via DEP, the cells are suspended in the sucrose medium for a certain period, leading to cell lysis. In addition, exposure of biological cells to electric fields can cause power dissipation and temperature increase in cell membranes [59]–[61]. In order to examine these effects with the current scaffold design, a series of experiments were conducted and the results from different experimental parameters were summarized in Fig. 11. Patterned cells were collected from the scaffolds, and cell viability was assayed using 0.4% Trypan Blue solution. Input voltages of 0 V (without DEP) and 10 V (with DEP) with 500 kHz for 10 min was selected as the two control groups. In the first set of the experiment, input voltages of 5, 10, and 20 V were considered and the results indicate that over 90% of cell viability can be achieved for input voltage of 10 V or below. However, as the input voltage increases to 20 V, the cell viability drops to 60%, as shown in Fig 11(a). The effect of patterning time was also investigated, and the DEP patterning time was set to 5, 10, and 20 min, respectively. After 5 min of DEP patterning, the cell viability was comparable to that of
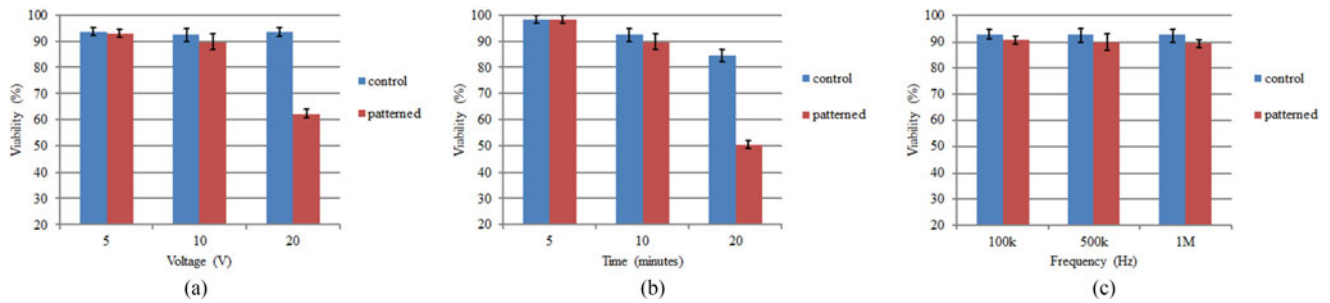
Fig. 11. (a) Assessment of MC3T3-E1 cell viability after DEP patterning with different voltages, (b) time, and (c) frequencies.

the control group [see Fig. 11(a)]. When DEP patterning was extended to 10 min, the cell viability decreased but remained above 90%. When the procedure was continued for 20 min, the cell viability decreased to only 50% [see Fig. 11(b)]. From the control group, an approximately 10% drop in the cell viability from 5 to 20 min also indicates that the use of sucrose medium also leads to cell death. Comparing the two data obtained from the 20-min test, cell death due to the DEP effect was more severe. One possible factor that caused the change in cell viability was the generation of temporary pores, also known as electroporation, on the cell membrane [62]. These pores allow the gradual uptake of molecules from the DEP buffer medium into viable cells, where large uptake of molecules is correlated with the loss of cell viability [63], [64]. The effect of the operating voltage frequency was also examined and no significant change in the cell viability was noticed, as shown in Fig. 11(c). Based on the results, the optimal setting for DEP patterning should be around 10 V and 10 min to minimize cell death.

D. Patterning Efficiency

The number of cells as patterned onto each layer of the scaffold high depends on the strength of the DEP force induced on the cells. As shown in (1), the strength is proportional to the square of the electric field gradient, and a higher voltage input can lead to denser cellular patterns constructed from the multilayer scaffold structure. In addition, with a higher voltage input, the cellular patterns could be formed within a shorter period and with better distribution [31]. In contrast, when a low or zero voltage is applied to the scaffold, majority of the cells could be sunk down to the bottom of the scaffold, covering the Petri dish's surface as illustrated in Fig. 12. Almost no cells could be adhered to the sidewalls of different scaffold layers. The presence of other cells can also affect the number of cells being manipulated by DEP. When more dielectric cells are placed in the microenvironment, the electric fields generated by the multilayer scaffold can be distorted. Therefore, regions that are relatively uniform originally can become more nonuniform because the nearby dielectric cells and DEP forces can be induced on the cells in these regions to promote cell patterning. To examine this effect, different cell concentrations were seeded onto the proposed scaffold. Fig. 13 illustrates the formation of the cellular patterns from three different cell concentrations through the DEP force. A voltage of 10 V with a frequency of 500 kHz was applied for 10 min for each test. When a medium with
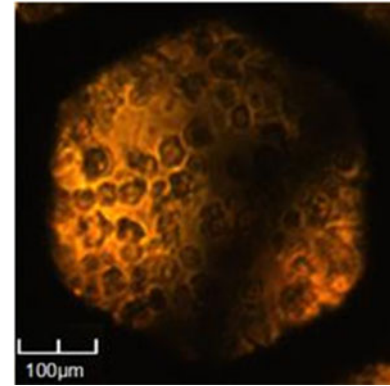

Fig. 12. Microscope image at the bottom of the scaffold with cells covering the surface of the Petri dish (0-V voltage input).

low cell concentration (4.5×10^4 cells/mL) was pipetted onto the scaffold, the structure was not fully covered by cells after DEP patterning [see Fig. 13(a)]. When a higher cell concentration medium (1.25×10^6 cells/mL) was pipetted, more cells were manipulated by DEP to construct the cellular patterns [see Fig. 13(b)]. Cells were adhered along the edges of the structure to construct more uniform honeycomb-like cellular patterns. Cell chains were formed under the DEP effect, and cellular patterns formed on the adjacent layers (out-of-focus). Increasing the concentration to 5×10^6 cells/mL produced denser cellular patterns. Excess cells accumulated and patterned on top of honeycomb-like cellular patterns [see Fig. 13(c)]. These excess cells did not adhere to the scaffold and could be washed away because of medium exchange. Thus, proper cell concentration should be used to minimize the use of cells in forming the necessary cellular patterns for culture.

To examine the effect of cell size on patterning, three types of cells with approximately the same concentration (1.25×10^6 cells/mL) were manipulated by DEP with the multilayer scaffold. These cells were labeled with MitoTracker Red to enhance the contrast between the background and the cellular pattern. A voltage input of 10 V was supplied to the scaffold, and cellular patterns were observed after 10 min, as shown in Fig. 14(a)–(f). Among the three types of cells, HFF had the largest diameter and the smallest number of cells patterned. One possible reason for this phenomenon is that these cells showed sufficiently increased resistance to pass through the interconnected pores toward the interior part of
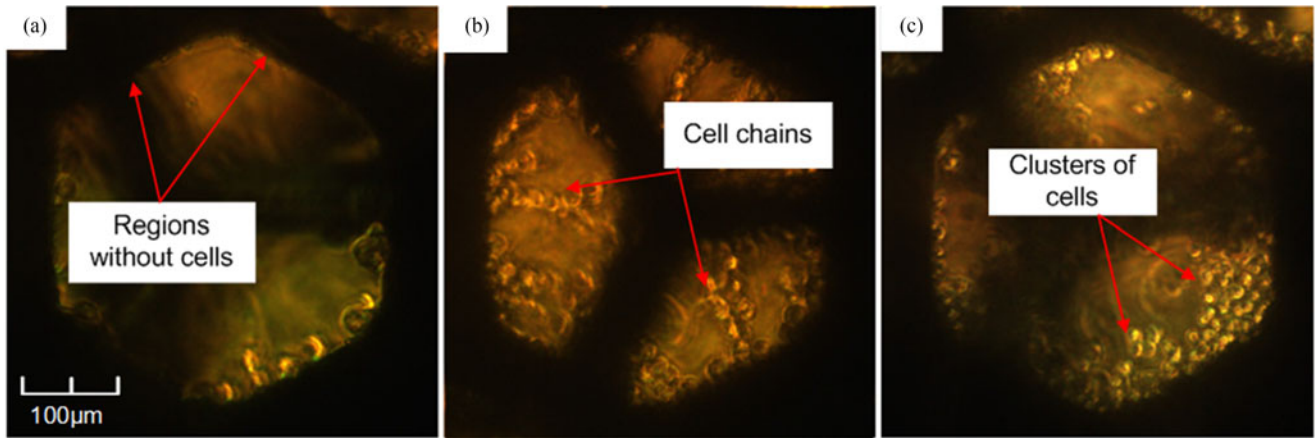
Fig. 13. Cellular patterns on the second scaffold layer with different cell concentrations: (a) 4.5×10^4 cells/mL, (b) 1.25×10^6 cells/mL, and (c) 5×10^6 cells/mL.
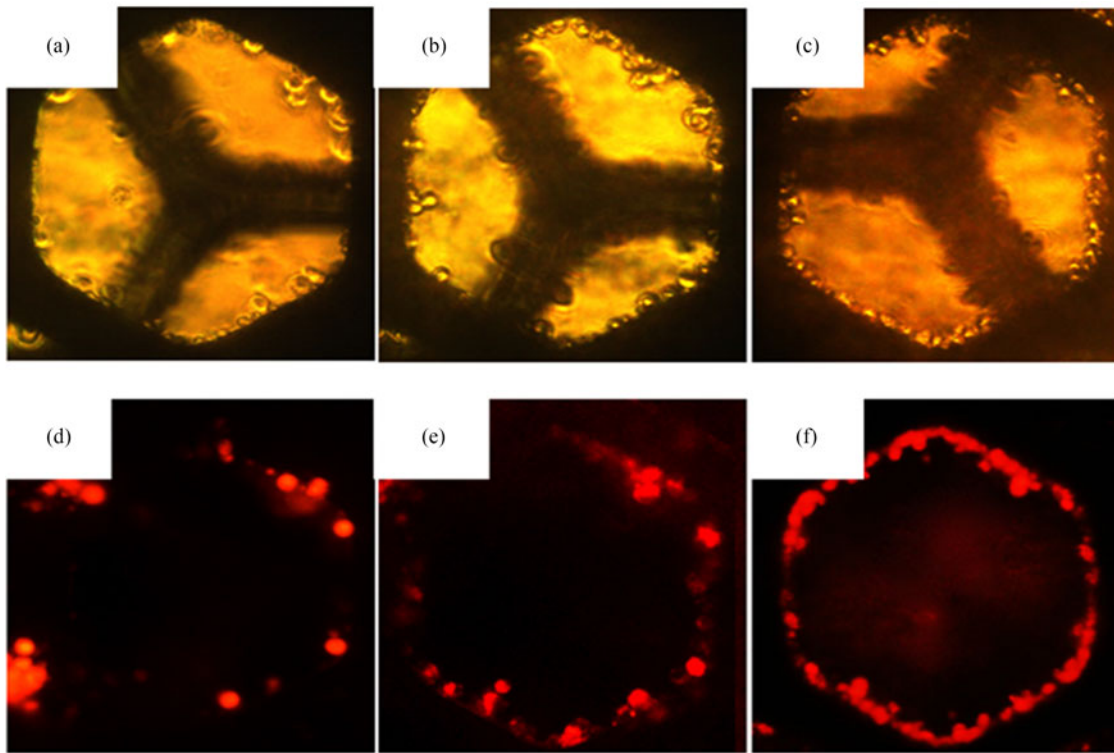

Fig. 14. Cellular patterns on the third scaffold layer with different types of cells: bright-field images for (a) HFF cells, (b) MC3T3-E1 cells, and (c) OCI-AML3 cells; fluorescent images for (d) HFF cells, (e) MC3T3-E1 cells, and (f) OCI-AML3 cells.

the scaffold. Thus, fewer cells were presented within the pores to construct the patterns, which were scarce. As the diameter of the cell type decreased, more cells passed through to form a pattern on the scaffold, as confirmed by the intensity from the fluorescent images. Leukemia cells, which have the smallest size, can achieve more homogeneous, honeycomb patterns. Hence, cell size can directly influence the formation of cellular patterns, and the geometric design of the interconnected pores should be adjusted accordingly for cells with larger diameters.

IV. CONCLUSION

A novel multilayer scaffold designed to mimic the 3-D geometry of a native tissue was proposed. While the conventional practice is unable to control the cells distributed on the scaffold, this scaffold utilized DEP as the mechanism to manipulate cells toward the intrinsic architecture of the scaffold, thereby forming honeycomb-like cellular patterns on different layers for culture. Experiments were conducted to examine the performance of proposed scaffold on seeding and patterning of cells. Computer simulations were performed to confirm the electric

field distribution as generated through the scaffold for DEP manipulation. The optimal operating frequency correlated with the selected cell type was simulated. The biocompatibility of the fabricated material was evaluated, and the change in the cell viability over different operating periods was assayed. Three types of mammalian cells were examined for patterning on the proposed scaffold, and the results showed that cell size and the cell concentration influenced the density of the constructed cellular patterns. On the basis of the experiments conducted, the proposed scaffold could be used to pattern a wide range of cells into honeycomb-like cellular structures. The integrated DEP-based cell patterning technique could enhance cell seeding for the development of high-quality artificial tissues.

REFERENCES

[1] T. A. Ahmed and M. T. Hincke, "Mesenchymal stem cell-based tissue engineering strategies for repair of articular cartilage," *Histol. Histopathol.*, vol. 29, no. 6, pp. 669–689, 2014.

[2] J. T. Krawiec and D. A. Vorp, "Adult stem cell-based tissue engineered blood vessels: A review," *Biomater.*, vol. 33, pp. 3388–3400, 2012.

[3] K. Rezwan *et al.*, "Biodegradable and bioactive porous polymer/inorganic composite scaffolds for bone tissue engineering," *Biomater.*, vol. 27, pp. 3413–3431, 2006.

[4] A. Seidi and M. Ramalingam, "Protocols for biomaterial scaffold fabrication," in *Integrated Biomaterials in Tissue Engineering*, M. Ramalingam *et al.*, Ed. Hoboken, NJ, USA: Wiley, 2012, pp. 1–23.

[5] L. A. Solchaga *et al.*, "A rapid seeding technique for the assembly of large cell/scaffold composite constructs," *Tissue Eng.*, vol. 12, no. 7, pp. 1851–1863, 2006.

[6] S. W. Rhee *et al.*, "Patterned cell culture inside microfluidic devices," *Lab Chip*, vol. 5, pp. 102–107, 2005.

[7] X. Yan and D. Sun, "Multilevel-based topology design and cell patterning with robotically controlled optical tweezers," *IEEE Trans. Control Syst. Technol.*, vol. 23, no. 1, pp. 176–185, Jan. 2015.

[8] E. Eriksson *et al.*, "A microfluidic device for reversible environmental changes around single cells using optical tweezers for cell selection and positioning," *Lab Chip*, vol. 10, pp. 617–625, 2010.

[9] X. Li *et al.*, "Design of a robust unified controller for cell manipulation with a robot-aided optical tweezers system," *Autom.*, vol. 55, no. 5, pp. 279–286, 2015.

[10] H. Chen and D. Sun, "Moving groups of microparticles into array with a robot-tweezers manipulation system," *IEEE Trans. Robot.*, vol. 28, no. 5, pp. 1069–1080, Oct. 2012.

[11] U. Mirsaidov *et al.*, "Optimal optical trap for bacterial viability," *Phys. Rev. E*, vol. 78, pp. 021910, 2008.

[12] S. Hu and D. Sun, "Automatic transportation of biological cells with a robot-tweezer manipulation system," *Int. J. Robot. Res.*, vol. 30, no. 14, pp. 1681–1694, 2011.

[13] X. Gou *et al.*, "Applying combined optical tweezers and fluorescence microscopy technologies to manipulate cell adhesions for cell-to-cell interaction study," *IEEE Trans. Biomed. Eng.*, vol. 60, no. 8, pp. 2308–2315, Aug. 2013.

[14] S. Miltenyi *et al.*, "High gradient magnetic cell separation with MACS," *Cytometry*, vol. 11, pp. 231–238, 1990.

[15] A. Ito *et al.*, "Medical application of functionalized magnetic nanoparticles," *J. Biosci. Bioeng.*, vol. 100, pp. 1–11, 2005.

[16] S. C. Hur *et al.*, "Deformability-based cell classification and enrichment using inertial microfluidics," *Lab Chip*, vol. 11, pp. 912–920, 2011.

[17] A. J. Mach *et al.*, "Automated cellular sample preparation using a centrifuge-on-a-chip," *Lab Chip*, vol. 11, pp. 2827–2834, 2011.

[18] H. O. Fatoyinbo *et al.*, "A high-throughput 3-D composite dielectrophoretic separator," *IEEE Trans. Biomed. Eng.*, vol. 52, no. 7, pp. 1347–1349, Jul. 2005.

[19] D. R. Albrecht *et al.*, "Photo-and electropatterning of hydrogel-encapsulated living cell arrays," *Lab Chip*, vol. 5, pp. 111–118, 2005.

[20] H. Tsutsui *et al.*, "Efficient dielectrophoretic patterning of embryonic stem cells in energy landscapes defined by hydrogel geometries," *Ann. Biomed. Eng.*, vol. 38, no. 12, pp. 3777–3788, 2010.

[21] T. Yasukawa *et al.*, "Micropatterning with different cell types by dielectrophoretic manipulation," in *Proc. Int. Symp. Micro-NanoMecatron. Human Sci.*, Nagoya, Japan, 2007, pp. 179–182.

[22] J. Ramón-Azcón *et al.*, "Gelatin methacrylate as a promising hydrogel for 3D microscale organization and proliferation of dielectrophoretically patterned cells," *Lab Chip*, vol. 12, pp. 2959–2969, 2012.

[23] C. T. Ho *et al.*, "Rapid heterogeneous liver-cell on-chip patterning via the enhanced field-induced dielectrophoresis trap," *Lab Chip*, vol. 6, pp. 724–734, 2006.

[24] C. T. Ho *et al.*, "Liver-cell patterning Lab Chip: Mimicking the morphology of liver lobule structure," *Lab Chip*, vol. 13, pp. 3578–3587, 2013.

[25] R. Z. Lin *et al.*, "Dielectrophoresis based-cell patterning for tissue engineering," *Biotechnol. J.*, vol. 1, pp. 949–957, 2006.

[26] P. Bajaj *et al.*, "Patterned three-dimensional encapsulation of embryonic stem cells using dielectrophoresis and stereolithography," *Adv. Healthcare Mater.*, vol. 2, pp. 450–458, 2013.

[27] M. A. Asnaghi *et al.*, "Bioreactors: Enabling technologies for research and manufacturing," in *Tissue Engineering*, 2nd ed., C. A. van Blitterswijk and J. de Boer Ed. New York, NY, USA: Elsevier, 2015, pp. 393–421.

[28] C. C. Wang *et al.*, "A biomimetic honeycomb-like scaffold prepared by flow-focusing technology for cartilage regeneration," *Biotechnol. Bioeng.*, vol. 111, pp. 2338–2348, 2014.

[29] K. Alvarez and H. Nakajima, "Metallic scaffold for bone regeneration," *Materials*, vol. 2, pp. 790–832, 2009.

[30] U. Hansen *et al.*, "The effect of strain rate on the mechanical properties of human cortical bone," *J. Biomech. Eng.*, vol. 130, pp. 011011:1–8, 2008.

[31] H. K. Chu *et al.*, "Three-dimensional cell manipulation and patterning using dielectrophoresis via a multi-layer scaffold structure," *Lab Chip*, vol. 15, pp. 920–930, 2015.

[32] Z. Huan *et al.*, "3D cell manipulation with honeycomb-patterned scaffold for regeneration of bone-like tissues," in *Proc. IEEE Int. Conf. Inf. Autom.*, Lijiang, China, 2015, pp. 1680–1685.

[33] H. A. Pohl, *Dielectrophoresis*. Cambridge, U.K.: Cambridge Univ. Press, 1978.

[34] C. P. Jen and T. W. Chen, "Selective trapping of live and dead mammalian cells using insulator-based dielectrophoresis within open-top microstructures," *Biomed. Microdevices*, vol. 11, pp. 597–607, 2009.

[35] R. Martinez-Duarte *et al.*, "A novel approach to dielectrophoresis using carbon electrodes," *Electrophoresis*, vol. 32, pp. 2385–2392, 2011.

[36] C. P. Jen *et al.*, "Three-dimensional focusing of particles using negative dielectrophoretic force in a microfluidic chip with insulating microstructures and dual planar microelectrodes," *Electrophoresis*, vol. 32, pp. 2428–2435, 2011.

[37] N. G. Green *et al.*, "Numerical solution of the dielectrophoretic and travelling wave forces for interdigitated electrode arrays using the finite element method," *J. Electrost.*, vol. 56, pp. 235–254, 2002.

[38] M. Nouri-Felekori *et al.*, "Development of composite scaffolds in the system of gelatin−calcium phosphate whiskers/fibrous spherulites for bone tissue engineering," *Ceram. Int.*, vol. 41, pp. 6013–6019, 2015.

[39] S. C. Cox *et al.*, "3D printing of porous hydroxyapatite scaffolds intended for use in bone tissue engineering applications," *Mater. Sci. Eng.: C*, vol. 47, pp. 237–247, 2015.

[40] Y. Zhu *et al.*, "Honeycomb-structured films by multifunctional amphiphilic biodegradable copolymers: Surface morphology control and biomedical application as scaffolds for cell growth," *ACS Appl. Mater. Interfaces*, vol. 3, pp. 2487–2495, 2011.

[41] H. Itoh *et al.*, "A honeycomb collagen carrier for cell culture as a tissue engineering scaffold," *Artif. Organs*, vol. 25, pp. 213–217, 2001.

[42] M. Sato *et al.*, "An atelocollagen honeycomb-shaped scaffold with a membrane seal (ACHMS-scaffold) for the culture of annulus fibrosus cells from an intervertebral disc," *J. Biomed. Mater. Res. Part A*, vol. 64, pp. 248–256, 2003.

[43] S. Deepthi *et al.*, "Fabrication of Chitin/Poly (butylene succinate)/Chondroitin sulfate nanoparticles ternary composite hydrogel scaffold for skin tissue engineering," *Polym.*, vol. 6, pp. 2974–2984, 2014.

[44] H. K. Cheung *et al.*, "Composite hydrogel scaffolds incorporating decellularized adipose tissue for soft tissue engineering with adipose-derived stem cells," *Biomaterials*, vol. 35, pp. 1914–1923, 2014.

[45] M. Martina and D. W. Hutmacher, "Biodegradable polymers applied in tissue engineering research: A review," *Polymer Int.*, vol. 56, pp. 145–157, 2007.

[46] V. K. Balla *et al.*, "Porous tantalum structures for bone implants: Fabrication, mechanical and in vitro biological properties," *Acta Biomaterialia*, vol. 6, pp. 3349–3359, 2010.

[47] M. Yazdimamaghani *et al.*, "Surface modification of biodegradable porous Mg bone scaffold using polycaprolactone/bioactive glass composite," *Mater. Sci. Eng.: C*, vol. *49*, pp. 436–444, 2015.

[48] H. Liu *et al.*, "Design and characterization of a conductive nanostructured polypyrrole-polycaprolactone coated magnesium/PLGA composite for tissue engineering scaffolds," *J. Biomed. Mater. Res. Part A*, vol. 103, pp. 2966–2973, 2015.

[49] M. M. Dewidar *et al.*, "Processing and mechanical properties of porous 316L stainless steel for biomedical applications," *Trans. Nonferr. Metals Soc. China*, vol. 17, pp. 468–473, 2007.

[50] C. M. Murphy *et al.*, "The effect of mean pore size on cell attachment, proliferation and migration in collagen–glycosaminoglycan scaffolds for bone tissue engineering," *Biomater.*, vol. 31, pp. 461–466, 2010.

[51] Q. Zhang *et al.*, "Pore size effect of collagen scaffolds on cartilage regeneration," *Acta Biomater.*, vol. 10, pp. 2005–2013, 2014.

[52] S. V. Puttaswamy *et al.*, "Enhanced cell viability and cell adhesion using low conductivity medium for negative dielectrophoretic cell patterning," *Biotechnol. J.*, vol. 5, pp. 1005–1015, 2010.

[53] S. Tavakol *et al.*, "Effect of laminated hydroxyapatite/gelatin nanocomposite scaffold structure on osteogenesis using unrestricted somatic stem cells in rat," *Cell Biol. Int.*, vol. 37, pp. 1181–1189, 2013.

[54] P. O. Bagnaninchi and N. Drummond, "Real-time label-free monitoring of adipose-derived stem cell differentiation with electric cell-substrate impedance sensing," *Proc. Nat. Acad. Sci. USA*, vol. 108, pp. 6462–6467, 2011.

[55] J. Chen *et al.*, "Classification of cell types using a microfluidic device for mechanical and electrical measurement on single cells," *Lab Chip*, vol. 11, pp. 3174–3181, 2011.

[56] J. E. Aubin and J. T. Triffitt, "Mesenchymal stem cells and osteoblast differentiation," in *Principles of Bone Biology*, 2nd ed., J. P. Bilezikian, L. G. Raisz, and G. A. Rodan Eds. New York, NY, USA: Academic, 2002, pp 59–82.

[57] H. Zhang *et al.*, "MC3T3-E1 cell response to stainless steel 316L with different surface treatments," *Mater. Sci. Eng. C*, vol. 56, pp. 22–29, 2015.

[58] D. M. Liu *et al.*, "Sol-gel hydroxyapatite coating on stainless steel substrates," *Biomaterials*, vol. 23, pp. 691–698. 2002.

[59] U. Zimmermann *et al.*, "Effects of external electrical fields on cell membranes," *Bioelectrochem. Bioenerg.*, vol. 3, pp. 58–83, 1976.

[60] T. Kotnik and D. Miklavčič, "Theoretical evaluation of the distributed power dissipation in biological cells exposed to electric fields," *Bioelectromagnetics*, vol. 21, pp. 385–394, 2000.

[61] U. Zimmermann *et al.*, "Cells with manipulated functions: New perspectives for cell biology, medicine, and technology," *Angew. Chem. Int. Ed. Engl.*, vol. 20, pp. 325–344, 1981.

[62] C. Huang *et al.*, "Single cell viability observation in cell dielectrophoretic trapping on a microchip," *Appl. Phys. Lett.*, vol. 104, no. 013703, 2014, pp. 1–5.

[63] P. Canatella *et al.*, "Quantitative studies of electroporation-mediated molecular uptake and cell viability," *Biophys. J.*, vol. 80, pp. 755–764, 2001.

[64] W. K. Neu and J. C. Neu, "Mechanism of Irreversible Electroporation in Cells: Insight from the Models," in *Irreversible Electroporation, Series in Biomedical Engineering*, B. Rubinsky Ed. Berlin, Germany: Springer-Verlag, 2010, pp. 85–122.

Zhijie Huan (S'14) received the B.S. degree from the Department of Precision Machinery and Instrumentation, University of Science and Technology of China, Hefei, China, in 2011. He is currently working toward the Ph.D. degree with the University of Science and Technology of China and City University of Hong Kong Joint Advanced Research Center, Suzhou, China.

His research interests include dielctrophoresis-based cell manipulation and patterning for bone tissue engineering.

Henry K. Chu (M'12) received the B.S. degree in mechanical engineering from the University of Waterloo, Waterloo, ON, Canada, in 2005, and the M.S. and Ph.D. degrees in mechanical and industrial engineering from the University of Toronto, ON, Canada, in 2007 and 2011.

After his graduation, he continued as a Postdoctoral Fellow at the University of Toronto and at the City University of Hong Kong, Hong Kong.He is currently an Assistant Professor at the Hong Kong Polytechnic University, Hong Kong. His research interests include robotic manipulation, vision-based control and automation, microsystem design, and tissue engineering.

Jie Yang received the B.S. degree from the Department of Physical Chemistry, Beijing University of Science and Technology, Beijing, China, in 1969.

He is currently a Professor in the Department of Precision Machinery and Precision Instrumentation at the University of Science and Technology of China, Hefei, China. He has led a research group focusing on robotics supported by the National Science Foundation of China and the 863 Projects. His research interests include intelligent robots, shape memory materials, and high-speed photography.

Dong Sun (F'15) received the bachelor's and master's degrees from Tsinghua University, Beijing, China, and the Ph.D. degree from the Chinese University of Hong Kong, Hong Kong.

He is currently a Chair Professor and the Head in the Department of Mechanical and Biomedical Engineering, City University of Hong Kong, Hong Kong. Before he joined the City University of Hong Kong in 2000, he was a Postdoctoral Researcher at the University of Toronto, Toronto, ON, Canada. His research interests include robot-aided cell manipulation, multirobot systems, and motion controls. He has served editorial boards for many international journals such as the IEEE TRANSACTIONS ON ROBOTICS and the IEEE/ASME TRANSACTIONS ON MECHATRONICS.